



# Enhancing Ni-SiO<sub>2</sub> catalysts for the carbon dioxide reforming of methane: Reduction-oxidation-reduction pre-treatment

Emma C. Lovell, Andrew Fuller, Jason Scott\*, Rose Amal

School of Chemical Engineering, the University of New South Wales, Sydney, NSW 2052, Australia



## ARTICLE INFO

### Article history:

Received 19 January 2016

Received in revised form 11 May 2016

Accepted 31 May 2016

Available online 5 June 2016

### Keywords:

Carbon dioxide reforming

Methane

Nickel catalyst

Pre-treatment

Reduction-oxidation-reduction

## ABSTRACT

The work presented here evaluated the impact of reduction-oxidation-reduction (ROR) pre-treatment on 5 and 10% Ni-SiO<sub>2</sub> as an efficient and inexpensive manner of enhancing catalysts for the carbon dioxide reforming of methane. Samples were reduced, oxidised and subsequently re-reduced, with the Ni deposit characteristics being analysed at each step. It was demonstrated that ROR treatment decreased the average Ni deposit size and altered the interaction between the Ni and SiO<sub>2</sub>, which significantly enhanced catalytic performance. ROR pre-treatment resulted in an increase in CH<sub>4</sub> conversion, most significantly for the 10% Ni-SiO<sub>2</sub> samples (from 57% to 69% at 800 °C) with comparable carbon formation between the reduced and ROR pre-treated samples. During 600 °C stability tests the 10% reduced samples deactivated, due to carbon build-up, after 3–4 h reaction time. In contrast, at 600 °C the ROR sample maintained stable conversion after 6 h over a 12 h time frame. Additionally, for all samples ROR pre-treatment resulted in a more stoichiometric H<sub>2</sub>/CO ratio. The reduction in both Ni deposit size and crystallinity increased conversion and selectivity. This derived from a greater active metal surface area for conversion as well as a decrease in the prevalence of methane decomposition and the reverse water gas shift reaction by influencing the desorption of CO and lowering the occurrence of bulk NiO. Ultimately, ROR pre-treatment provides a simple and inexpensive means of improving dry reforming catalysts.

© 2016 Elsevier B.V. All rights reserved.

## 1. Introduction

The pervasive challenges of society's energy future have prompted considerable research to secure a more sustainable approach. The dry reforming of methane (DRM) offers a potential solution by utilising two of the most destructive greenhouse gases; methane and carbon dioxide. These gases are reacted to produce synthesis gas ( $CH_4 + CO_2 \rightarrow 2CO + 2H_2$ ,  $\Delta H = 247 \text{ kJ/mol}$ ) which can be used to produce both long chain hydrocarbons through the Fischer-Tropsch reaction and oxygenates. Despite the desirable environmental implications, the implementation of DRM catalysts on an industrial scale is limited by cost and stability. Highly active and stable catalysts for DRM have been reported however they generally consist of expensive noble metals [1,2] or complex structures [3–5]. The use of mesoporous supports facilitates active site dispersion resulting in desirable catalytic properties, however they typically require significant time in an autoclave, pH adjustments and multiple processing steps [3–5]. Ni catalysts provide a viable cost to performance trade-off, however their use is limited by their

inferior activity and stability [4,6,7]. Thus, research has recently focused on the development of Ni-based catalysts which have enhanced activity and stability comparable to noble metal catalysts.

Commercially feasible catalysts for DRM have limited stability, which is attributed to the tendency of carbon formation and sintering due to high reaction temperatures [8,9]. Carbon formation arises from methane decomposition as well as the Boudouard reaction at lower temperatures. To improve the catalytic properties, altering the type, acid-base properties and oxygen mobility of the support [10–13] as well as controlling the nickel particle size and distribution through preparation methods have been investigated [14–18]. In the >10 nm range, Ni size and distribution has been shown to have a significant impact on the activity and stability of Ni catalysts for the DRM [19–21]. Small Ni sizes with strong metal-support interaction have been proven to facilitate enhanced conversion, promoting a greater number of active sites available for conversion, as well as suppressing carbon formation. Despite this, the impact of the varying Ni size and metal support interaction on the selectivity of DRM catalysts is yet to be thoroughly understood.

Controlling Ni size and distribution on a silica support has been studied by utilising plasma technologies [20], and various precursors (resulting in the formation of difficult to reduce hydrosilicates) [22]. A method to vary active site size without the use of expen-

\* Corresponding author.

E-mail address: [jason.scott@unsw.edu.au](mailto:jason.scott@unsw.edu.au) (J. Scott).

sive precursors and complex synthesis techniques is desirable. Employing a reduction-oxidation-reduction (ROR) treatment process during the catalyst activation stage can alter metal catalyst deposit size while satisfying both these requirements. For instance, ROR was explored as a method of activating a cobalt catalyst for the Fischer-Tropsch reaction [23]. After ROR pre-treatment the Co species were re-dispersed resulting in the formation of smaller Co deposits with stronger metal-support interaction [23]. Unmuth et al. [24] reported that ROR pre-treatment resulted in a reduction in Ni deposit size for Ni-SiO<sub>2</sub> samples although the particles were not used for any subsequent reaction. Recently, Tang et al. [25] reported an increase in dispersion for Ru-Co/Al<sub>2</sub>O<sub>3</sub> supports with ROR pre-treatment which resulted in an increase in CO conversion for the Fischer-Tropsch reaction.

Given smaller Ni deposits are considered to be more favourable for DRM and in light of the ROR observations by Unmuth et al., the potential exists for ROR treatment to have a positive impact on the DRM. The study detailed here investigates using ROR treatment as a simple, inexpensive, and in-situ means of promoting DRM activity in Ni-based catalysts. Herein, silica is utilised as the support due to its facilitation of a high degree of Ni reduction as well as its neutral acidity/basicity [26]. Ni-SiO<sub>2</sub> samples at varying Ni levels were either reduced or ROR treated in-situ and characterised with X-ray diffraction (XRD), transmission electron microscopy (TEM), H<sub>2</sub> and CO temperature programmed desorption (H<sub>2</sub>/CO-TPD) and H<sub>2</sub> temperature programmed reduction (H<sub>2</sub>-TPR). The changes in Ni size and structure and metal-support interaction were then evaluated in terms of their impact on the DRM, particularly in reference to the effect on catalyst selectivity.

## 2. Experimental

### 2.1. Catalyst preparation

Ni-SiO<sub>2</sub> samples were prepared with 5 and 10 wt.% nominal Ni loadings using Davisil Grade 646 silica (Sigma-Aldrich, >99%) as the support. Actual Ni loadings were determined from inductively coupled plasma optical emission spectroscopy (ICP-OES) and differed from the nominal loading by <20%. Aqueous nickel nitrate precursor, Ni(NO<sub>3</sub>)<sub>2</sub>·6H<sub>2</sub>O (Sigma Aldrich, >98.5%), was added to a silica suspension (0.1 M), mixed for 3 h and then dried for 16 h at 100 °C. The samples were subsequently calcined in a fixed bed glass reactor (10 mm ID) under 60 mL/min of air (Coregas Dry Compressed Air) for 4 h at 450 °C with a 5 °C/min ramp rate. Bulk NiO was synthesised as a basis for reduction temperature comparison during H<sub>2</sub>-TPR studies. To produce the bulk NiO, nickel nitrate (Ni(NO<sub>3</sub>)<sub>2</sub>·6H<sub>2</sub>O) was calcined for 4 h at 450 °C with a 5 °C/min ramp rate.

### 2.2. Catalyst activity

Catalytic activity for DRM was assessed using the apparatus displayed in Fig. S1 and as outlined in [27]. Typically, 25 mg of catalyst was diluted with 25 mg of silica (Fluka, Silica Gel 40, surface area = 522 m<sup>2</sup>/g) and loaded into a quartz reactor (6 mm ID, 300 mm long) between two plugs of quartz wool. A thermocouple was positioned within the reactor tube just above the catalyst bed, and the entire system was then placed in a tube furnace. All activity tests were conducted at atmospheric pressure.

Catalyst performance was assessed in terms of: (i) light-off profiles and; (ii) 12 h stability tests. Prior to the activity tests samples were either reduced or ROR pre-treated. Catalyst reduction involved holding the sample at 350 °C (1 °C/min ramp rate) for 10 h under 60 mL/min of 50% H<sub>2</sub>/Ar (Coregas Hydrogen, >99.99%; Coregas Argon, >99.992%). During activation via ROR, the catalyst was

reduced as above after which it was oxidised under 60 mL/min of air at 300 °C (1 °C/min ramp rate) for 2 h (details on identifying the ideal re-oxidation conditions can be found in Supporting Information). The second reduction step then involved exposing the re-oxidised sample to 50% H<sub>2</sub>/Ar (60 mL/min) for 10 h at 275 °C (1 °C/min ramp rate). Following activation (reduction or ROR) the catalysts were cooled to room temperature under Ar (60 mL/min).

When generating light-off curves, the activated samples were heated under 60 mL/min N<sub>2</sub> (Coregas Nitrogen, >99.999%) to 500 °C (5 °C/min) and held for 1 h. A reactant gas mix with a 1:1:1 ratio of CH<sub>4</sub>:CO<sub>2</sub>:N<sub>2</sub> (Coregas Methane, >99.95%; Coregas Carbon Dioxide, >99.99%) was introduced to the catalyst bed at a weight hourly space velocity (WHSV) of 144 L/(h·g<sub>cat</sub>). After the gases had stabilised, the system was retained at 500 °C for a further 0.5 h during which the composition of the reactor effluent was analysed. The reactor was subsequently heated in 50 °C increments (at 5 °C/min) to 800 °C with a 0.5 h hold at each step with the gas composition evaluated at each temperature step. During the 12 h stability tests the activated catalyst was heated under 60 mL/min N<sub>2</sub> (Coregas Nitrogen, >99.999%) to 600 °C (5 °C/min) and held for 0.25 h. Gases were then introduced in the same ratio and WHSV as above and the system retained at 600 °C for 12 h with the reactor effluent monitored over this period. The stability test was conducted at 600 °C to minimise the impact of carbon formation from the Boudouard reaction (2CO → CO<sub>2</sub> + C) at lower temperatures. Mears' and Weisz-Prater criterion were calculated along with initial experiments which confirmed that heat and mass transfer limitations are avoided within the system (see Supporting Information 1.1 for details). Control tests with the diluent silica (not shown) displayed negligible conversion at 800 °C.

Gases were analysed with two online gas chromatographs (GC) in parallel; a Shimadzu 8A with a thermal conductivity detector (TCD) and Molecular Sieve 13X column for H<sub>2</sub> and N<sub>2</sub> detection and a Shimadzu 2010 with a flame ionisation detector (FID) and HP/Plot Q column for CH<sub>4</sub>, CO<sub>2</sub> and CO detection. A cold trap with ice was located between the reactor outlet and GC inlets to remove any moisture which may have been generated from the reverse water gas shift (RWGS, CO<sub>2</sub> + H<sub>2</sub> ⇌ CO + H<sub>2</sub>O) side reaction.

### 2.3. Characterisation

To decrease the potential for Ni re-oxidation of the reduced and ROR-treated samples prior to XRD and TEM characterisation the samples were passivated using the catalytic apparatus (Fig. S1). Following reduction or ROR treatment the samples were cooled to room temperature under Ar (60 mL/min) and then passivated. To understand the impact of the heat treatment time on Ni deposit properties a control sample was prepared. 10% Ni-SiO<sub>2</sub> was held in 50% H<sub>2</sub>/Ar mixture for 34 h and 45 min (the same total heating time as the ROR samples including ramping time) prior to being passivated. Passivation involved passing 40 mL/min of 0.5% O<sub>2</sub> in He (Linde 0.9% O<sub>2</sub> – He balance; Coregas Helium, >99.996%) through the catalyst bed for 8 h at room temperature. Passivated samples are denoted as R/P or ROR/P.

Ni crystal size was examined using XRD (PANalytical Xpert Multipurpose X-ray Diffraction System). The sample was loaded onto a no-background sample holder and scanned with a CuK $\alpha_1$  radiation ( $\lambda = 0.154$  nm) at 45 kV and 40 mA from 10 to 80° at 0.067°/s. The Ni and NiO crystal sizes were estimated from the Scherrer equation ( $d(nm) = \frac{0.9 \cdot \lambda}{\beta \cdot \cos\theta}$ , where  $\beta$  is full width at half maximum and  $\theta$  is the Bragg angle). TEM images were captured on a FEI Tecnai G2 20 at 200 kV with the samples dispersed in methanol prior to imaging. For Ni deposit size calculations at least 300 Ni particles were measured.

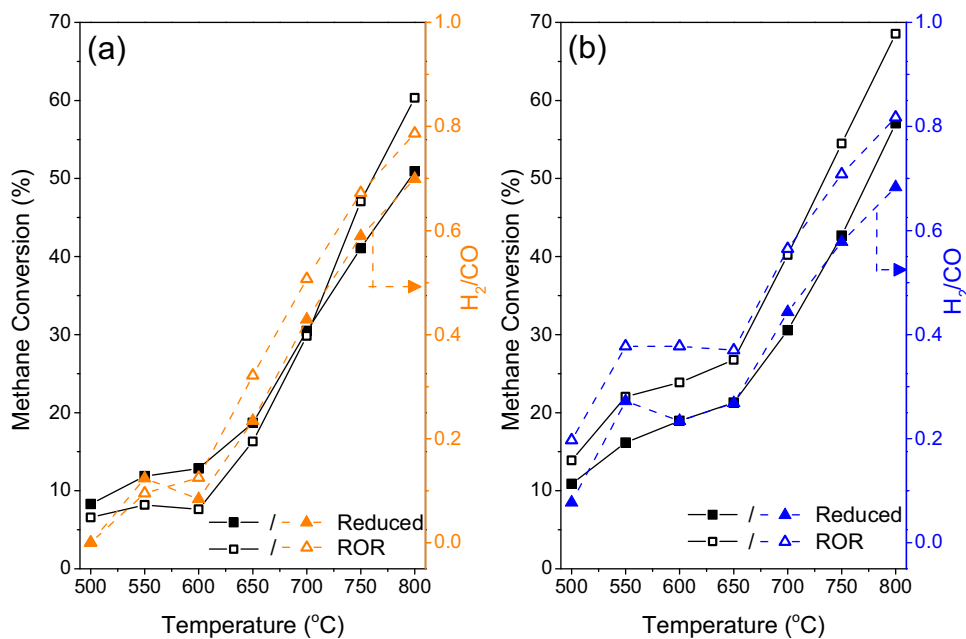


**Fig. 1.** Methane light-off curves and accompanying  $\text{H}_2/\text{CO}$  product ratio during methane reforming by  $\text{CO}_2$  for (a) 5% and (b) 10% Ni-SiO<sub>2</sub>. Conditions: WHSV = 144 L/(h g<sub>catalyst</sub>), catalyst loading = 0.025 g,  $\text{N}_2:\text{CH}_4:\text{CO}_2$  = 1:1:1.

Inductively-coupled plasma optical emission spectroscopy (ICP-OES) was used to determine the actual Ni loadings for dispersion calculations. Samples were partially digested with concentrated aqua regia and heating for 3 h at 90 °C. The samples were left overnight to digest and then diluted with milli-Q water to 10 mL whereby they were analysed using a Perkin Elmer OPTIMA 7300.

$\text{H}_2$ -TPR studies were conducted on an AutoChem II 2920 system with a TCD. Approximately 50 mg of sample was pre-treated at 150 °C (ramp rate 10 °C/min) for 30 min under Ar (Coregas Argon, >99.999%) and then cooled to 50 °C. The samples were heated from 50 °C to 900 °C at a rate of 5 °C/min under 5%  $\text{H}_2$  in Ar (10%  $\text{H}_2$  in Ar diluted by Ar; Coregas) with a flow rate of 20 mL/min. For RO-TPR experiments, the samples were reduced and oxidised in the dry reforming rig (Fig. 1), transferred to the AutoChem and then subjected to the  $\text{H}_2$ -TPR procedure detailed above. Hydrogen temperature-programmed desorption ( $\text{H}_2$ -TPD) studies were also conducted on the AutoChem II 2920 to evaluate Ni dispersion. Typically 50 mg of sample was reduced or ROR pre-treated in-situ. After pre-treatment the samples were cooled in 50%  $\text{H}_2$ /Ar (flow rate = 20 mL/min) and held at 50 °C for 2 h to allow Ni surface coverage by the  $\text{H}_2$ . The sample was then degassed in 100% Ar (flow rate = 20 mL/min) for 2 h to remove physisorbed  $\text{H}_2$  before heating (5 °C/min) to 300 °C. Dispersion was calculated from [28,29] with dispersion (%) =  $(100 \times \text{H}_2 \text{ uptake} \times \text{Ni atomic weight} \times \text{stoichiometry}) / (\text{Ni fraction})$ , where  $\text{H}_2$  uptake was taken as molar volume of  $\text{H}_2$  adsorbed per mass on Ni present and a stoichiometry of 2 surface Ni: 1  $\text{H}_2$  being assumed [30].

Carbon on the spent samples was characterised by thermogravimetric analysis (TGA). For the TGA experiments approximately 2 mg of sample was heated in a Pt sample holder to 800 °C under air (Coregas Dry Compressed Air, 100%) using a TA instruments TGA Q5000.

### 3. Results and discussion

#### 3.1. Catalyst activity, stability and carbon accumulation

Light-off curves comparing the impact of reduction and ROR activation on the Ni-SiO<sub>2</sub> catalysts for the DRM reaction were gen-

erated over the temperature range 500 °C–800 °C and are provided in Fig. 1. Also presented in Fig. 1 is the change in  $\text{H}_2/\text{CO}$  ratio in the product stream over the same temperature range. The light-off curves are typical of the DRM reaction given its endothermic nature [31] and are characterised by two regimes: (i) a comparatively low increase in methane conversion with temperature over the range 500 °C–600/650 °C (depending on Ni loading); (ii) a markedly higher extent of methane conversion with temperature over the range 600/650 °C to 800 °C. The  $\text{H}_2/\text{CO}$  ratio exhibits a similar profile to the methane conversion, increasing at a greater rate from 600/650 °C onward, although remaining below one across all studied temperatures.

The methane conversion and  $\text{H}_2/\text{CO}$  profiles are governed by the prevalence of the DRM reaction and the associated side reactions (i.e. Boudouard, RWGS and methane decomposition). The  $\text{H}_2/\text{CO}$  ratio is typically used to indicate the selectivity of catalysts for the DRM. A ratio of approximately one implies a balance between all side reactions in terms of  $\text{H}_2$  and CO production/consumption [26]. The Boudouard reaction ( $2\text{CO} \rightarrow \text{C} + \text{CO}_2$ ) and methane decomposition ( $\text{CH}_4 \rightarrow \text{C} + 2\text{H}_2$ ) result in carbon formation and a rise in the  $\text{H}_2/\text{CO}$  ratio. The RWGS ( $\text{CO}_2 + \text{H}_2 \rightarrow \text{CO} + \text{H}_2\text{O}$ ) results in water formation and a reduction in the  $\text{H}_2/\text{CO}$  ratio. A  $\text{H}_2/\text{CO}$  ratio of less than one indicates the prominence of the RWGS reaction within the system, which consumes valuable  $\text{H}_2$  and  $\text{CO}_2$ . As observed in Fig. 1, the  $\text{H}_2/\text{CO}$  ratio remains below one across the temperature range considered indicating the prevalence of the RWGS, although the value varies with temperature. Below 650 °C the Boudouard reaction (which increases the  $\text{H}_2/\text{CO}$  ratio through CO consumption) is thermodynamically favourable although the low  $\text{H}_2/\text{CO}$  ratio at this temperature indicates any related CO consumption is significantly offset by the RWGS reaction. Beyond 650 °C the Boudouard reaction is no longer favourable while the likelihood of methane decomposition and the RWGS reaction increases linearly with temperature [12]. The increase in  $\text{H}_2/\text{CO}$  ratio with increasing temperature indicates methane decomposition becomes the increasingly dominant side reaction, counteracting the  $\text{H}_2$  consumption by the RWGS reaction.

When comparing light-off curves for the reduced and ROR pre-treated samples, it is apparent the degree of impact of ROR pre-

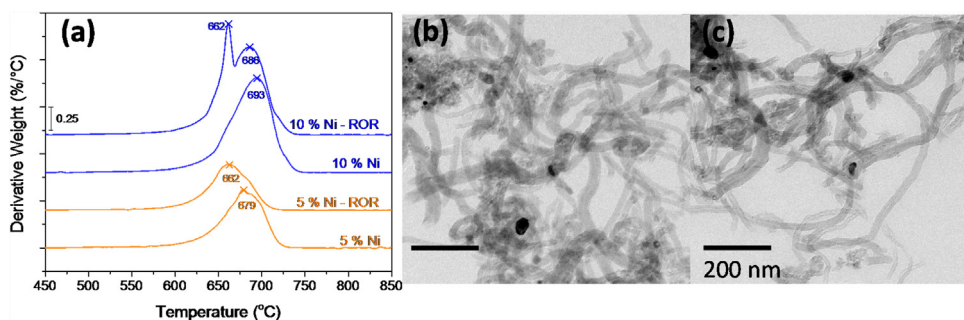


**Fig. 2.** (a) Derivative carbon oxidation weight profiles for 5% and 10% Ni-SiO<sub>2</sub> with reduction or ROR pre-treatment after incremental temperature activity tests. TEM images of spent 10% Ni-SiO<sub>2</sub> catalysts following (b) reduction and (c) ROR pre-treatment showing filamentous carbon accumulation during the DRM process.

treatment is a function of the Ni loading (Fig. 1). In the case of the 5% Ni-SiO<sub>2</sub> sample, there does not appear to be a distinct effect of ROR treatment on the CH<sub>4</sub> conversion or H<sub>2</sub>/CO ratio, especially at lower temperatures where the low conversion (<15%) means the error margins are greater. In contrast, ROR treatment of the 10% Ni-SiO<sub>2</sub> catalyst improves methane conversion across all temperatures as well as consistently lifting the H<sub>2</sub>/CO ratio, by a value of around 0.1, indicating a decrease in selectivity towards the RWGS reaction. The impact of ROR treatment seems to be more distinct for the higher Ni loading perhaps due to the larger quantity of Ni and the greater initial presence of the larger Ni deposits leading to a greater potential to redisperse after ROR treatment.

Carbon accumulation during the DRM light-off tests was probed using the derivative carbon weight loss (with temperature) and TEM images of the spent catalysts as displayed in Fig. 2. The extent of carbon accumulation during the light-off tests for the 10% Ni loading (reduced = 12.7 mg<sub>carbon</sub>/L<sub>CH4converted</sub>, ROR = 10.6 mg<sub>carbon</sub>/L<sub>CH4converted</sub>) was approximately triple that of the 5% Ni loading (reduced = 4.1 mg<sub>carbon</sub>/L<sub>CH4converted</sub>, ROR = 3.4 mg<sub>carbon</sub>/L<sub>CH4converted</sub>) and is attributed to the greater Ni content. In addition, ROR pre-treatment decreased the quantity of carbon accumulated by ~17% for both Ni loadings and, as illustrated by Fig. 2 (a), to some extent it altered the nature of the formed carbon. The reduced 10% Ni-SiO<sub>2</sub> profile is characterised by a dominant peak with a maxima at 693 °C and contains a small shoulder on the lower temperature side. The ROR-treated 10% Ni-SiO<sub>2</sub> sample presents a similar dominant peak (maxima 686 °C) with a second sharp peak occurring at the lower temperature of 662 °C. The 5% Ni-SiO<sub>2</sub> catalyst exhibits similar features although not as distinct as the 10% Ni-SiO<sub>2</sub> sample. The TEM images (Fig. 2(b)) and (c)) indicate the accumulated carbon is filamentous for both reduced and ROR pre-treated samples. Filamentous carbon does not directly deactivate the catalyst, however over time it can result in reactor blocking [32,33]. Attempts to identify the origin of the new peak introduced by ROR were unsuccessful although it is believed at this time the peak derives from a second form of carbon. It shows the impact of ROR treatment is again more extensive for the higher Ni loading. No readily apparent difference between the accumulated carbon characteristics based on the two pre-treatment strategies is evident from the TEM images with this discussed in greater detail at a later time.

Catalyst stability or proclivity to deactivate with time was evaluated for the two activation strategies with the different Ni loadings. Methane conversion and the H<sub>2</sub>/CO ratio during 12 h of the DRM reaction at 600 °C are shown in Fig. 3. Included in the Figure (as insets) is the carbon formed (as mg<sub>carbon</sub>/L<sub>CH4converted</sub>) over the 12 h period. The methane conversion profiles for the 5% Ni-SiO<sub>2</sub> catalyst (Fig. 3(a)) are characterised by an initial decrease in activity to almost zero after approximately three hours of run time with the activity then recovering slightly to stabilise at approximately 3%

from seven hours onwards. Apart from an initially higher methane conversion for the ROR-treated sample, the profiles exhibit similar values over the 12 h. The H<sub>2</sub>/CO ratios for both pre-treatments also decrease with time, reaching a value close to zero after 6–7 h, indicating any small amount of H<sub>2</sub> being produced by the reforming (and/or cracking) reaction is consumed by the RWGS reaction.

The 10% Ni-SiO<sub>2</sub> samples also undergo deactivation with time (Fig. 3(b)) although not as rapidly as for the 5% Ni-SiO<sub>2</sub> sample. Methane conversion by the ROR-treated sample is initially ~32% (at 0.5 h) where it decreases at a roughly constant rate to reach a minimum (~2%) after 6 h. Beyond 6 h the activity partially recovers to stabilise at approximately 7%. Initial methane conversion by the reduced sample is slightly lower (~29%) and decreases with time whereby, between 3 and 4 h, the reaction ceased due to reactor blockage, presumably from filamentous carbon build up. The initial H<sub>2</sub>/CO ratio for the ROR-treated catalyst is higher than the 5% Ni-SiO<sub>2</sub> sample and remains stable for the first hour. From two hours to five hours the ratio declines after which it begins to level off to around a value of 0.1. The H<sub>2</sub>/CO ratio for the reduced 10% Ni-SiO<sub>2</sub>

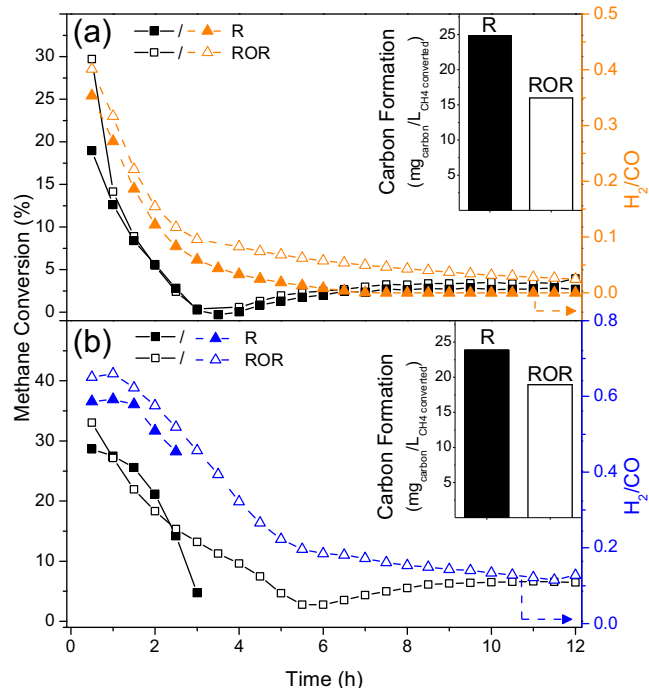


**Fig. 3.** Change in CH<sub>4</sub> conversion and H<sub>2</sub>/CO ratio with time for (a) 5% and (b) 10% Ni-SiO<sub>2</sub> at 600 °C comparing the impact of R and ROR pre-treatment (WHSV of 144 L/(h·g<sub>cat</sub>), catalyst loading = 0.025 g, 1:1 N<sub>2</sub>:CH<sub>4</sub>:CO<sub>2</sub>). Inset shows carbon formation in (mg<sub>carbon</sub>/L<sub>CH4converted</sub>) as determined by TGA (CH<sub>4</sub> input = 16.8 × 10<sup>-3</sup> mol/h).

catalyst follows a similar path up to 3 h, whereby no further data was attainable due to reactor blockage. Over the 3 h though, the ratio is consistently lower than for the ROR-treated catalyst and again illustrates ROR-treatment restricts the RWGS reaction.

Upon evaluating the carbon formed during the stability test, it was again observed that ROR treatment lowered the accumulation at both Ni loadings (Fig. 3 insets). The difference in carbon accumulation was around 35% and 25% for the 5% and 10% Ni loadings, respectively, which is larger than the difference observed for the light-off profiles (~17%). The difference may be attributed to the stability tests being run solely at 600 °C where the Boudouard reaction is thermodynamically favourable over the reaction period as opposed to the light of curves where methane decomposition dominates carbon formation above 650 °C [12]. Additionally, within the ROR samples, the 5% Ni results in less total carbon compared to the 10% sample, despite the relative carbon formation values being comparable. As more methane is converted the relative quantity of carbon was equivalent between the 5 and 10% loadings, however the total carbon formed over the 10% samples was 40–55% higher than the 5% samples. This can be attributed to the reduced amount of active surface Ni available for conversion. For the reduced samples, deactivation of the 10% sample within 3–4 h means that the carbon formed over the 12 h was underestimated, although the early reaction termination due to reactor blockage implies this sample is more susceptible to coking than the 5% Ni-SiO<sub>2</sub>.

The activity, stability and carbon accumulation findings each indicate ROR treatment has a positive impact on the catalyst performance for the DRM reaction. The extent of the benefit appears to be a function of the Ni loading and the reaction conditions. The impact of ROR treatment on the 5% Ni loaded sample in terms of improving activity and altering the prevalence of side reactions was difficult to discern, although differences in carbon accumulation indicated some effect was evident. In the instance of the 10% Ni loading the effect of ROR treatment was more tangible where it suppressed the RWGS reaction irrespective of the reaction temperature or reaction time. ROR treatment also decreased the extent of carbon accumulation (at a set temperature) with time as well as partially altered the nature of the formed carbon, suggesting a lower tendency towards the Boudouard reaction. The propensity for DRM and the associated side reactions to occur is governed by various catalyst attributes with Ni dispersion and support interaction being two key elements. The ensuing section probes these characteristics to understand the benefits imposed by ROR treatment on the DRM reaction.

### 3.2. Ni crystallinity, size and dispersion

XRD was used to map variations in the Ni/NiO crystallinity for the 5% and 10% Ni-SiO<sub>2</sub> catalysts throughout the stages of the ROR activation process. Fig. 4(a) provides the XRD spectra for the calcined (Ni) and reduced and re-oxidised (Ni-RO) samples, while Fig. 4(b) contains the XRD spectra for the reduced (R/P) and ROR-treated (ROR/P) samples after passivation. The oxidised Ni materials and the reduced Ni catalysts have been grouped within the two separate Figures in this instance to allow for easier evaluation of the effect re-oxidation and re-reduction has on the NiO and Ni deposit characteristics.

The XRD profiles in Fig. 4(a) exhibit peaks at 2θ values of 44, 52 and 76° which can be referenced to NiO(111), NiO(200) and NiO(220) positions, respectively (ICSD collection code 44767). There is no evidence of any metallic Ni remaining after calcining or RO treatment. The 2θ = 44.5, 51.9 and 76.4° peaks for all samples in Fig. 4(b) represent Ni(111), Ni(200) and Ni(220) reflections, respectively (ICSD collection code 44767). There is no evidence of any NiO remaining after reduction or ROR treatment. It is apparent passivation has been successful at protecting the Ni metal from re-oxidation while not subjecting it to extensive re-oxidation. The

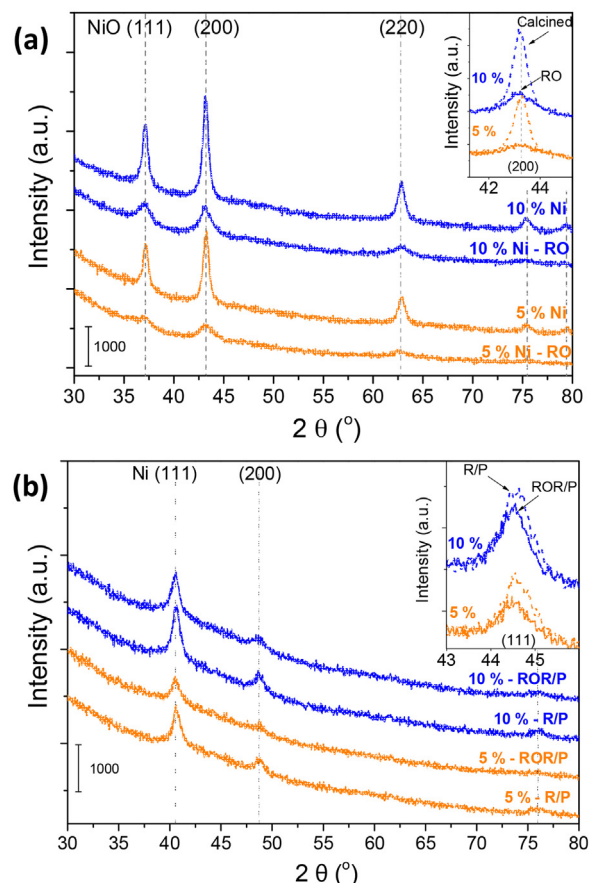


**Fig. 4.** XRD patterns of Ni-SiO<sub>2</sub> catalysts containing 5% and 10% Ni loadings after calcination. (a) As prepared and reduction and re-oxidation (Ni-RO) pre-treated; (b) reduction and passivation (R/P) and ROR treatment and passivation (ROR/P). The insets compare: (a) the NiO(200) reflections; (b) the Ni(111) reflections arising from the pre-treatments for the two Ni loadings.

pre-treated and passivated samples were utilised for TEM studies as well. The decreasing baseline in Fig. 4a and b is residual from the significant tailing of the characteristic amorphous silica peak at 22° (not shown) [34].

Upon considering the Ni-SiO<sub>2</sub> profiles for both Ni loadings in Fig. 4(a), the RO treatment decreases the intensity of the NiO reflections compared with the calcined particles. The broader peaks exhibited by the re-oxidised material signify the RO treatment has induced a decrease in the NiO crystallite size with the values, as estimated using the Scherrer Equation, provided in Table 1. The extent to which the RO treatment decreases NiO peak intensity is highlighted by the inset (for the NiO(200) reflection) in Fig. 4(a).

When contrasting the XRD profiles for the reduced samples (Fig. 4(b)) a similar effect is observed, whereby the second reduction step also decreases the full width half maxima values of the Ni reflections. The extent of the decrease is illustrated by the accompanying inset in Fig. 4(b), with the corresponding estimates for the Ni crystallite sizes provided in Table 1. The relative reduction in Ni crystal size (based on the Ni(111) reflection) arising from the two reduction pre-treatments was greater for the 10% Ni loading (18%) than the 5% Ni loading (5%) indicating ROR treatment has a more pronounced effect at the higher Ni loading.

While XRD was suitable for evaluating Ni/NiO crystallinity, TEM was used to assess Ni/NiO deposit size to gain a greater appreciation of the Ni deposit make-up. TEM micrographs of the 5% Ni-SiO<sub>2</sub> and 10% Ni-SiO<sub>2</sub> samples at each stage of the ROR treatment process are provided in Fig. 5(a) and (b), respectively. Included in Fig. 5

**Table 1**

Ni and NiO crystallite size, deposit size and dispersion values during the various stages of ROR pre-treatment.

Ni Loading	Pre-Treatment	Ni Size (nm)		Ni Span (from TEM)	Change in dispersion <sup>b</sup>	Ni size ratio post reaction <sup>c</sup>
		XRD <sup>a</sup>	TEM			
5%	calcined	11.7	17.6	1.80	n.a.	n.a.
	R <sup>d</sup>	10.0	12.3	1.68	n.a.	2.7
	RO	4.2	10.5	1.66	n.a.	n.a.
	ROR <sup>d</sup>	9.5	10.8	1.84	1.10	1.9
	calcined	12.8	22.2	2.81	n.a.	n.a.
	R <sup>d</sup>	10.3	12.4	1.83	n.a.	2.7
10%	RO	5.8	13.3	2.01	n.a.	n.a.
	ROR <sup>d</sup>	8.7	10.5	1.75	1.10	2.2

n.a. not available.

<sup>a</sup> Calculated from the Scherrer equation using XRD profiles from the Ni(111).

<sup>b</sup> Dispersion of ROR sample/dispersion of reduced sample.

<sup>c</sup> Calculated from the Scherrer equation using XRD profiles comparing Ni (200) reflection before and after incremental temperature activity test.

<sup>d</sup> Samples were passivated prior to characterisation.

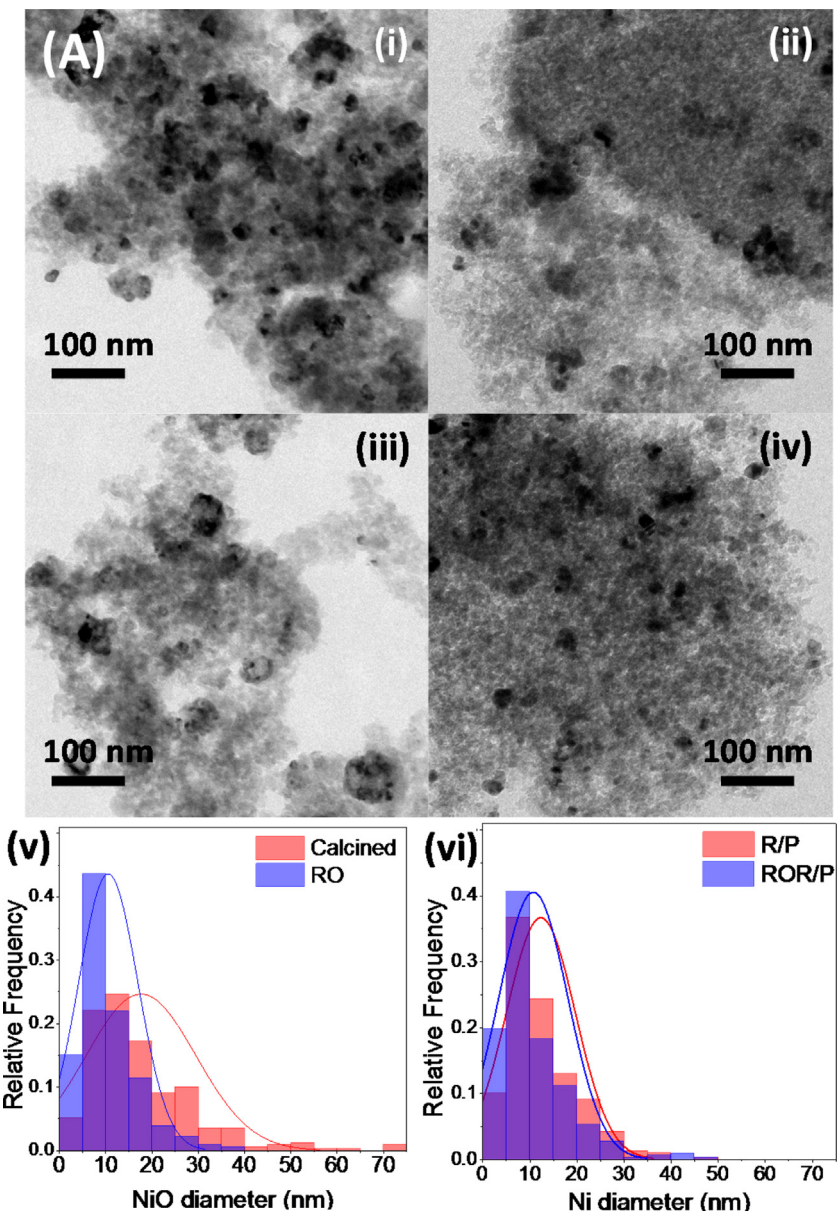


**Fig. 5.** TEM micrographs of (A) 5 and (B) 10% Ni-SiO<sub>2</sub> samples following: (i) calcination; (ii) reduction(R/P); (iii) reduction and re-oxidation (RO); and (iv) ROR/P treatment. Included are NiO/Ni deposit size distributions ( $n > 300$ ) evaluated using the TEM micrographs comparing the: (v) calcined and RO-treated; (vi) reduced and ROR-treated samples with lines showing normal distribution curves. Purple indicates the overlap between two samples.

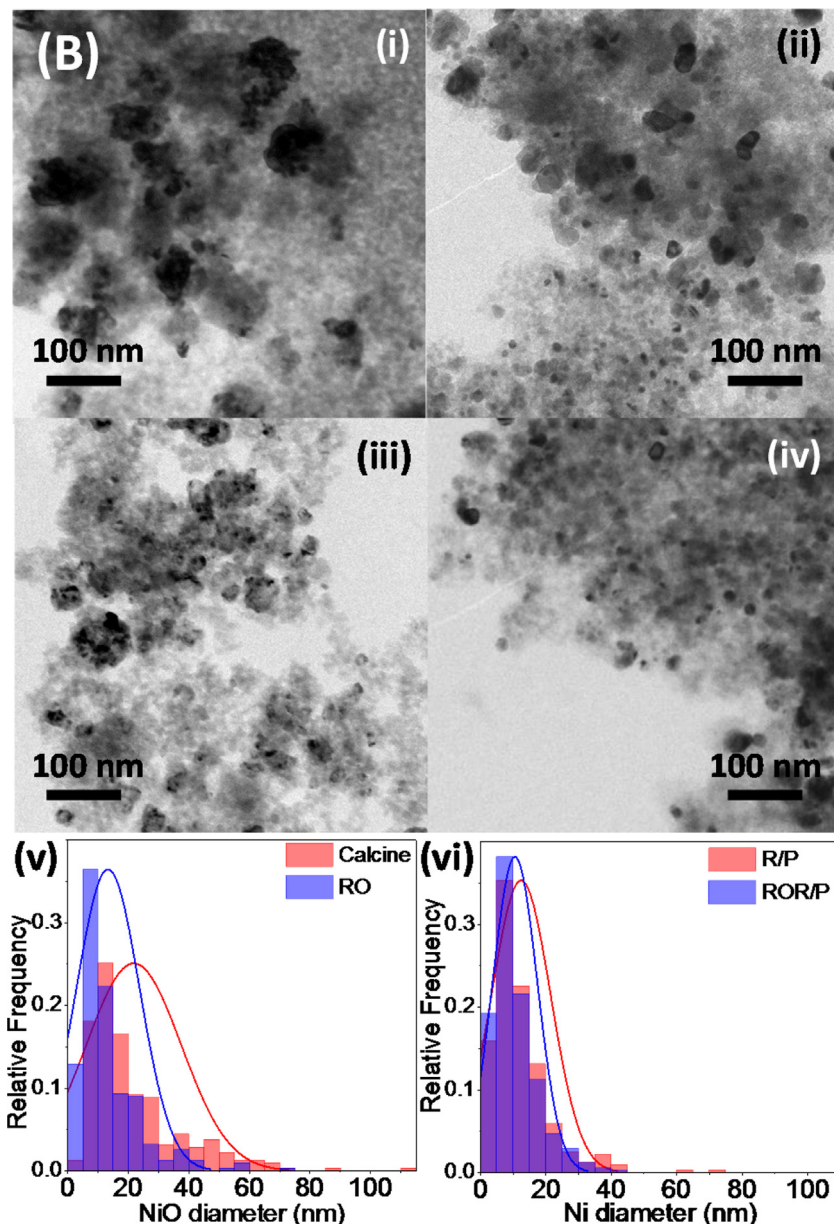


Fig. 5. (Continued)

are the associated Ni deposit size distributions following each of the oxidation/reduction stages. TEM images for the two Ni loadings both indicate there are differences in the features of the NiO and Ni deposits following the treatment steps. NiO deposits on the calcined and RO samples appear to be dominated by groupings of smaller NiO crystallites, with this effect more apparent for the 10% Ni-SiO<sub>2</sub> catalyst. The grouping effect does not seem to be as prevalent for the RO-treated sample with the Ni crystallites appearing to be more dispersed. The degree of crystallite grouping appears to decline during each of the reduction steps. The cluster sizes appear smaller and there is an increased number of isolated Ni crystallites, particularly for the 10% Ni-SiO<sub>2</sub> sample.

The size distribution profiles extracted from the TEM images conform to the XRD findings, with the RO and ROR steps decreasing the NiO/Ni sizes relative to the calcined and reduced samples, respectively. The average sizes, as given in Table 1, are comparable to the values derived from XRD. As well as a decrease in NiO/Ni deposit size, the TEM images show the deposit size distribution decreases with each subsequent treatment stage. The broadness of

a size distribution can be semi-quantitatively defined by its span (see Supporting Information Section 3) with the span values estimated for each of the treatment steps being provided in Table 1. At both Ni loadings the initial reduction step provides the greatest reduction in span and is more pronounced for the 10% Ni-SiO<sub>2</sub> catalyst. The reduction in distribution span when coupled with the decrease in average deposit size indicates an increase in NiO/Ni deposit dispersion.

The length of treatment time for the ROR pre-treatment, compared to the reduction treatment, may result in a change in Ni size due to time at elevated temperatures. To examine this an extended heat-treatment time, R-HT/P (reduced-heat-treated and passivated) 10% Ni-SiO<sub>2</sub>, sample was prepared. The results from XRD and TEM (see Supporting Information Section 4) show no significant change in Ni deposit size after the extended heat treatment time (<5% difference compared to the R/P sample). This indicates that the relatively mild conditions of the pre-treatments (275–350 °C compared to the 450 °C calcination and 500–800 °C activity testing) do not significantly impact the deposit properties

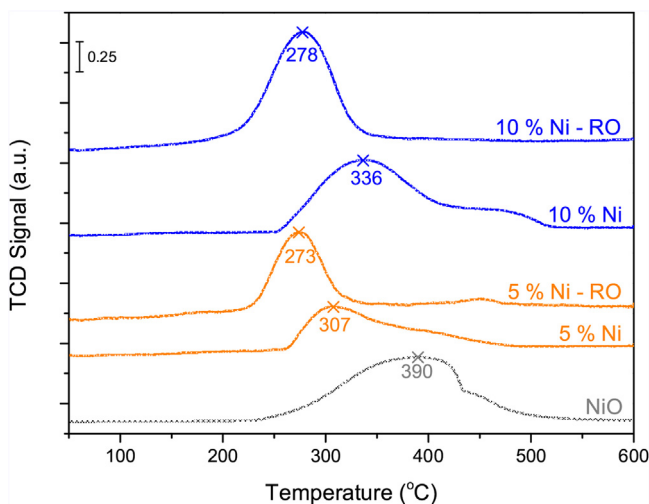


**Fig. 6.**  $\text{H}_2$  – TPR profiles for calcined (Ni) and re-oxidised (RO) 5% and 10% Ni- $\text{SiO}_2$  catalysts. Included for comparison is the  $\text{H}_2$  – TPR profile for  $\text{NiO}$  produced in-house ( $\text{Ni}(\text{NO}_3)_2 \cdot 6\text{H}_2\text{O}$  calcined at  $450^\circ\text{C}$  for 4 h).

and thus the changes in Ni characteristics can be attributed solely to the ROR treatments.

$\text{H}_2$ -TPD was utilised to further examine the impacts of the ROR pre-treatment on Ni dispersion. The results indicated that ROR treatment increases Ni dispersion (Table 1), agreeing with the evaluations from the TEM images. The  $\text{H}_2$ -TPD analysis indicated the Ni deposit dispersion increased by approximately 10% between the reduction and ROR stages.

### 3.3. Ni Deposit – $\text{SiO}_2$ support interaction

Characterisation to this point has indicated ROR treatment impacts on the size and dispersion of the Ni/ $\text{NiO}$  deposits without providing any information on whether the treatment alters deposit interaction with the  $\text{SiO}_2$  support.  $\text{H}_2$ -TPR was used to assess whether there was an impact of ROR treatment on deposit-support interaction with the reduction profiles for the calcined and re-oxidised 5% and 10% Ni- $\text{SiO}_2$  samples provided in Fig. 6. The  $\text{H}_2$ -TPR profile for  $\text{NiO}$  powder was included for comparison. The reduction profiles of the calcined samples are characterised by a primary reduction peak (peak maxima at  $307^\circ\text{C}$  and  $336^\circ\text{C}$  for the 5% and 10% Ni loadings, respectively) coupled with a broad, higher temperature shoulder. The broad shoulder occurs in a temperature region similar to the bulk  $\text{NiO}$  maximum suggesting the interaction between these particular  $\text{NiO}$  deposits and the  $\text{SiO}_2$  support is weak. Occurrence of the more dominant peak at a lower temperature suggests these deposits interact more strongly with the  $\text{SiO}_2$  support with the peak assigned to representing smaller, well-dispersed  $\text{NiO}$  species.

Fig. 6 shows that RO treatment impacts on the interaction between the  $\text{NiO}$  deposits and the  $\text{SiO}_2$  support for both Ni loadings. RO-treatment alters the reduction profiles to provide a single dominant peak at a comparatively lower temperature (between  $270^\circ\text{C}$  and  $280^\circ\text{C}$  for both Ni loadings) than was present for the calcined samples. The lower reduction temperature indicates RO treatment invokes a stronger interaction between the  $\text{NiO}$  deposits and the support and the (effective) loss of the higher temperature shoulder suggests a re-dispersion of the 'bulk-like'  $\text{NiO}$  deposits has occurred. The  $\text{H}_2$ -TPR results indicate that as the 10% Ni- $\text{SiO}_2$  sample had the largest quantity of bulk  $\text{NiO}$  available for re-dispersion on the silica. As there is more bulk  $\text{NiO}$  available, the 10% sample was able to facilitate a greater degree of re-dispersion, which is consistent with the results presented in Section 3.2.

A positive outcome of the stronger Ni deposit  $\text{SiO}_2$  support interaction induced by the ROR treatment is a decrease in the extent of Ni crystallite sintering during reaction. The factor by which the Ni crystallite size increased during the incremental temperature activity study was assessed by comparing the Ni(200) reflections from XRD spectra taken prior to (Fig. 4) and post (Supporting Information, Fig. S7) reaction, with the values provided in Table 1. A 35% reduction in Ni crystal size (as estimated from the Scherrer equation and XRD reflections) after ROR pre-treatment, coupled with a change in the structure of the Ni deposits, and the manner in which they interact with the support resulted in significant variations in catalytic performance. Both the 5% and 10% Ni- $\text{SiO}_2$  catalysts exhibit a decrease in the extent of Ni deposit sintering during reaction illustrating the stronger support-metal deposit interaction shown in the earlier  $\text{H}_2$ -TPR profiles (Fig. 6).

### 3.4. Discussion

The activity and stability findings indicated that ROR treatment generally improved Ni- $\text{SiO}_2$  catalytic performance while the characterisation studies revealed a decrease in Ni deposit/crystallite size and an increase in the deposit-support interaction strength. Given the impact was more pronounced for the higher (10%) Ni loading, presumably because of the greater initial presence of the larger bulk  $\text{NiO}$  deposits following calcination (i.e. the sample will be more sensitive to future changes in Ni deposit size), the ensuing discussion will primarily focus on this particular catalyst.

As summarised in Table 1, it is evident that ROR pre-treatment results in a reduction in Ni size. This reduction is most evident for higher Ni loading, with the 10% sample showing 10–15% decrease in Ni size and a clear change in Ni deposit structure. The exact mechanism of this change in deposit characteristics is unknown however it has been postulated that after reduction, oxidation causes an agglomeration of the Ni species resulting in a larger  $\text{NiO}$  species with increased coverage of the support [24]. The larger  $\text{NiO}$  redisperses when re-reduced resulting in the presence of smaller Ni. To study this phenomenon, XRD, TEM and  $\text{H}_2$ -TPR of the reduced and oxidised samples were completed and compared to the calcined samples.

Interestingly, the results indicate that the reduced and re-oxidised samples have smaller  $\text{NiO}$  sizes than the as-prepared samples, as represented in the Schematic below (Fig. 7). Unnuth et al., attributed the particle size reduction of Co- $\text{Al}_2\text{O}_3$  to an increase in support wetting and decrease in Ni crystallinity after RO treatment [24]. However, Mile et al. [35] found that after reduction and re-oxidation, their Ni- $\text{SiO}_2$  samples did not show any significant changes compared to the parent oxide which contradicts the findings from this study. Their study utilised a mesoporous silica material, perhaps preventing the migration and dispersion of the nickel across the support during oxidation. In our case the reduction in  $\text{NiO}$  size is consistent with the XRD showing a reduction in Ni size. Thus the proposed mechanism of Ni deposit size change during ROR pre-treatment of the Ni- $\text{SiO}_2$  samples is shown in Fig. 7, whereby after reduction, oxidation promotes the formation of smaller, significantly less crystalline  $\text{NiO}$  deposits (in comparison to the calcined samples). The smaller  $\text{NiO}$  deposits, when re-reduced, result in the formation of Ni with higher dispersion across the support. This study establishes the application of ROR pre-treatment beyond the already reported Co- $\text{Al}_2\text{O}_3$  for the Fischer-Tropsch reaction. The results from Mile et al. demonstrate that if the metal for re-oxidation is bound too strongly to the support surface (in their case within a porous  $\text{SiO}_2$  structure) then the ROR pre-treatment will not allow sufficient migration during oxidation and therefore subsequent re-dispersion is ineffective [35]. From this work and the literature, it can be postulated that ROR pre-treatment can be utilised on a range of supported metal oxide catalysts, beyond Co-

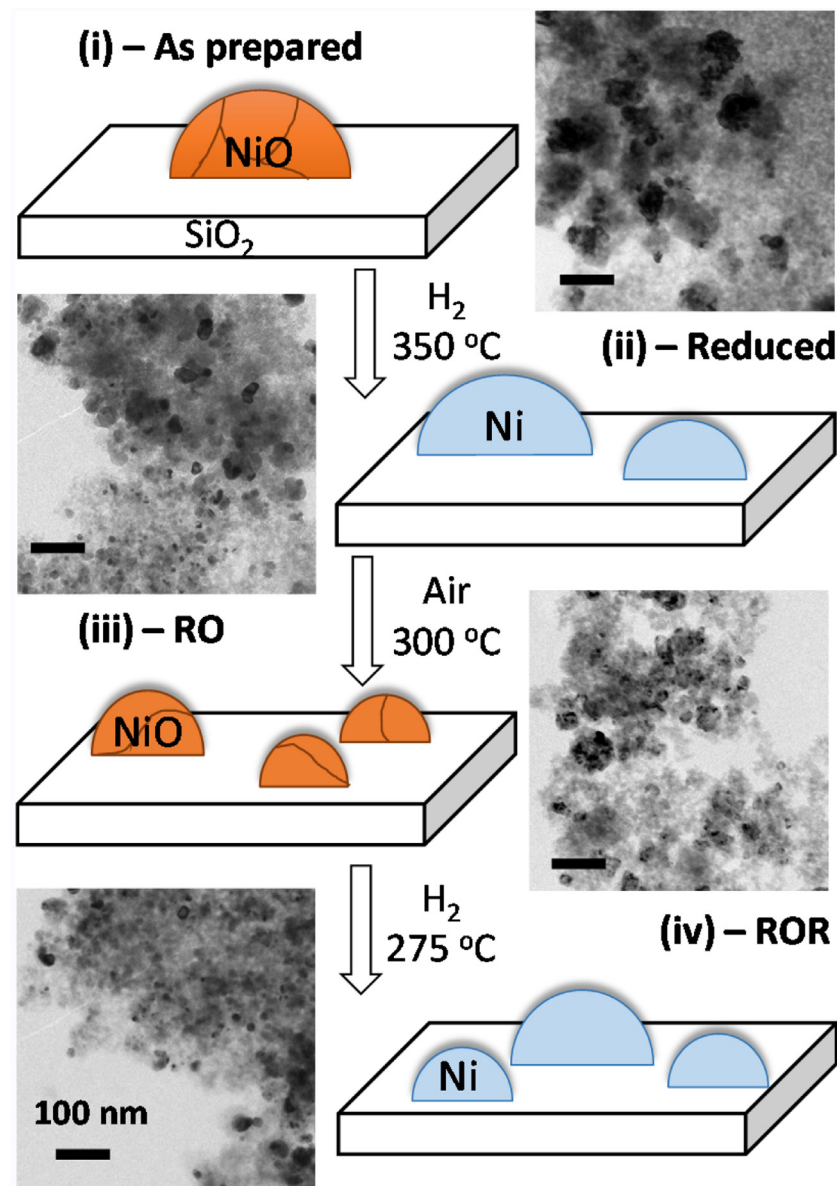


**Fig. 7.** Schematic of ROR phenomena proposed by the study from XRD, TEM and  $\text{H}_2$ -TPR results with TEM micrographs of 10% Ni-SiO<sub>2</sub> samples following: (i) calcination; (ii) reduction(R/P); (iii) reduction and re-oxidation (RO); and (iv) ROR/P treatment.

$\text{Al}_2\text{O}_3$  and Ni-SiO<sub>2</sub>. The application of ROR pre-treatment appears to be limited to materials where the metal-support interaction is not too strong to prevent the metal migration on the support surface.

Increasing Ni loading results in an increase in both the bulk NiO and reducible Ni present on the silica (evidenced by the increasing area under the  $\text{H}_2$ -TPR curve (Fig. 6)). Ni disperses on the support surface until the stronger adsorption sites are saturated and subsequently bulk NiO begins to form with low metal-support interaction. For the 5 and 10% Ni loadings a reduction in peak temperature as well as a narrowing of reduction peak resulted from the RO pre-treatment. After oxidation the peak shifted to approximately 275 °C with one sharp peak present, unlike the calcined samples with a shoulder evident. The peak shift and lack of a bulk NiO shoulder is indicative of the formation of smaller, more dispersed Ni species. The finding corroborates the XRD results, implying a reduction in Ni size from ROR pre-treatment. Further, for both 5 and 10% Ni-SiO<sub>2</sub> the peak area after RO pre-treatment is >90% of the original calcined sample thus confirming the sufficient oxidation of the Ni.

For supported Ni samples it is generally accepted that an increased reduction temperature is representative of stronger metal-support interactions [20,36]. However, in the case of Cu a lower reduction temperature is representative of smaller more dispersed Cu [37]. When considering that ROR pre-treatment results in smaller, more dispersed Ni (XRD and TEM) it follows that there will be increased metal-support interaction. Additionally, after reaction the ROR samples exhibit less sintering further indicating that this lowering in reduction temperature is caused by an increase in metal support interaction. The Scherrer equation was utilised to examine the change in Ni size after incremental temperature activity tests. ROR pre-treatment results in a significantly smaller increase in Ni crystal size after reaction (Table 1) indicating less sintering during reaction. The smaller crystal size is expected as the previous TEM and XRD results indicate that ROR pre-treatment reduces Ni deposit size and increases metal-support interaction (evidenced from TPR) resulting in less sintering.

The decrease in Ni deposit size and accompanying increase in dispersion (Table 1) from ROR treatment is presumed (in part at

least) to be responsible for the increased methane conversion displayed by the 10% Ni-SiO<sub>2</sub> catalyst (Fig. 1b). The ensuing increase in active surface area provides more sites for methane decomposition and the dissociative adsorption of CO<sub>2</sub> which provides a higher intrinsic activity [14–18]. In contrast, there is no distinct benefit of increased dispersion on methane conversion for the 5% Ni-SiO<sub>2</sub>, indicating the active surface area alone is not the sole contributor to catalyst performance. The low loading and resulting low conversion means the effects on activity and carbon coking are not obvious compared to the 10% sample. The higher loading sample facilitates high enough activity that the differences in conversion and coking are observable. Baudouin et al. [38] reported a similar result to our 5% Ni-SiO<sub>2</sub> catalyst whereby the DRM was independent of Ni size and dispersion in the range of 1.6–7.3 nm. The study found that with a Ni loading of 0.9–18.5% (and in the aforementioned size range), the intrinsic activity and selectivity of the DRM catalysts were independent from size and dispersion. For this study (within the 8–13 nm range) it is evident that size plays an intricate role in the reaction mechanism. The 5% reduced samples show high carbon formation and higher deactivation over the duration of the tests, particularly at lower temperatures. This indicates that the 5% sample is more susceptible to carbon formation through the Boudouard reaction (discussed further below).

Variations in the H<sub>2</sub>/CO ratio, carbon accumulation and deposit-support interaction suggest the improved dispersion from ROR treatment provides other complementary/competing effects. The H<sub>2</sub>/CO ratio is, for the most, elevated by the ROR treatment (Fig. 1) and remains higher over an extended reaction period (Fig. 3). An increase in H<sub>2</sub>/CO ratio can arise from any of the following; an increase in prominence of methane cracking, an increase in the Boudouard reaction or a suppression of the RWGS reaction. The carbon oxidation profiles (Fig. 2) showed that ROR treatment does not increase the quantity of carbon formed (generally the ROR pre-treatment resulted in a reduction in carbon formation). This suggests that the ROR pre-treatment does not promote methane cracking or the Boudouard reaction but helps to suppress the RWGS reaction. Suppressing the RWGS reaction results in a more stoichiometric H<sub>2</sub>/CO ratio suitable for downstream processing. The reduced samples do not show higher CO<sub>2</sub> conversion than the ROR pre-treated samples (CO<sub>2</sub> conversion not shown). Hence, the alteration of the structure of the ROR pre-treated Ni has a significant impact on adsorption/desorption properties of the reactants, intermediaries (CH<sub>x</sub>, CH<sub>x</sub>O, O, H) and/or products.

In this case the lower H<sub>2</sub>/CO ratio is from a relatively higher CO production for the reduced samples. XRD and TEM results have shown that ROR pre-treatment alters the size and structure of the Ni deposits (refer to Table 1) significantly. This is further emphasised by the variation in selectivity and activity after ROR pre-treatment (Figs. 1 and 3). The conversion rate (Fig. S5, methane conversion per Ni surface area) is higher for the ROR pre-treated samples for both 5 and 10% Ni loadings. This indicates that the decrease in Ni size, and increase in Ni surface area, from ROR pre-treatment was not the only factor that influenced the enhancement in methane conversion for the dry reforming reaction. It is well known that CH<sub>4</sub> decomposition as well as CO<sub>2</sub> dissociative adsorption is structure sensitive [20,39]. Therefore, as a result of the proven variation in Ni structure, the adsorption and desorption properties of the reactants and products would be significantly altered by the ROR pre-treatment. The lower H<sub>2</sub>/CO ratio suggests for ROR pre-treated samples have a lower tendency to promote the adsorption of CO<sub>2</sub> and/or a greater inclination to promote the desorption of CO. According to the dry reforming reaction mechanism, an increase in CO<sub>2</sub> dissociative adsorption would result in an increase in surface CO<sub>ads</sub> and O<sub>ads</sub> species. If this is the case, the build-up of surface species would result in a reduction in conversion. Additionally, an accumulation of surface CO promotes the Boudouard reaction and

an increase in O<sub>ads</sub> species promotes the RWGS by reacting with formed H<sub>2</sub>. CO-TPD (Fig. S3) was used to probe with CO adsorption strength between the reduced and ROR samples with the reduced samples showing stronger adsorption strength of CO in comparison to ROR pre-treated samples.

There is a distinct impact of ROR pre-treatment on the activity and selectivity of the prepared samples. This impact is further evident when examining the differences in carbon formation between the as-prepared and ROR pre-treated samples. This difference in carbon formation is highlighted both in the constant temperature tests with respect to quantity of carbon produced as well as in the incremental temperature activity tests in terms of the structure of the carbon.

For the constant temperature activity tests more significant differences in carbon formation are evident. Whilst the reduced and ROR samples show similar conversions, the ROR pre-treatment results in a significant reduction in carbon formation from 25 to 16 mg<sub>Carbon</sub>/L<sub>CH4,converted</sub> for the 5% Ni sample and 24 to 19 mg<sub>Carbon</sub>/L<sub>CH4,converted</sub> for the 10% sample. As aforementioned the reaction for the 10% sample ceased after 3–4 h whereas the ROR pre-treated sample continued converting for 12 h. This would undoubtedly have an impact on carbon formation, however this impact was offset by normalising the carbon formation to the total methane converted. Table S4 (Supporting Information) displays the average rate and selectivity of carbon formed through the 12 h tests. For the non-pre-treated samples, it follows that more carbon will be formed on the reduced samples due to their larger particle size and greater CO adsorption strength. This can be attributed to the reduction in bulk NiO, shown above, which promotes methane decomposition resulting in carbon formation.

For the incremental temperature activity tests, the total amount of carbon on the spent samples is similar for both R and ROR samples. The ROR pre-treated samples have higher methane conversion and therefore ROR facilitates lower carbon formation per methane conversion. The derivative weight curves show that ROR pre-treatment results in the formation of two carbon species; oxidation at approximately 665 °C and 685 °C. It is generally accepted that lower temperature oxidation carbon is amorphous carbon and the higher temperature peak is representative of crystalline carbon nanotubes [12,40]. Raman, XPS (Fig. S8 and S9), XRD (Fig. S7) and TEM (Fig. S6) did not show a significant difference in the carbon present on reduced and ROR pre-treated samples. Additionally, the temperature difference between the two peaks is relatively small (unlike those previously reported [12,40]). One possible explanation of this observation is that the difference in oxidation temperatures arise from variations in carbon nanotube diameter. TEM was used to obtain a size distribution for the diameter of the carbon nanotubes, (Fig. S6). The average diameter for carbon nanotubes present on the reduced and ROR pre-treated samples were 26 and 22 nm respectively. It is known that the diameter of the multi-walled carbon nanotubes formed from the metal-catalysed decomposition of methane is dependent on the metal particle size [41,42]. None of the measured carbon nanotubes have diameters less than 10 nm. This is in good agreement with previous studies, suggesting that 10 nm is the approximate limit for carbon formation avoidance [43,44]. The distribution of nanotube diameters (and reduction in average nanotube size) corresponds with the reduction in Ni size from ROR pre-treatment. Additionally, it would follow that the oxidation temperature of the formed nanotubes would be dependent on their diameters. From this, and the lack of structural difference in the formed carbon species, it can be speculated that variation in oxidation temperature arises from a difference in nanotube diameter.

Overall it is evident that ROR pre-treatment alters Ni deposit size, structure and metal-support interaction. By reducing the deposit size and increasing the active site surface area, ROR pre-

treatment enhance methane conversion significantly. The variation in deposit characteristics (including structure and metal-support interaction) alters the adsorption and desorption properties of the reactants and intermediaries and ultimately impacts the selectivity and stability of the catalysts.

#### 4. Conclusions

The findings demonstrate that ROR pre-treatment has a significant impact on Ni-SiO<sub>2</sub> catalysts for DRM. By ROR pre-treating samples the nature of the active Ni species changes significantly. Compared to reduced samples, ROR pre-treated samples show smaller, more highly dispersed Ni with altered metal-support interaction. The change in Ni deposit size has significant impacts on the DRM system, including conversion, stability and selectivity. The increase in conversion, particularly evident for the 10% Ni sample, can be attributed to the increase in active metallic surface area caused by the ROR pre-treatment. Additionally, ROR pre-treatment results in a more stoichiometric H<sub>2</sub>/CO ratio, which is desirable for downstream processing. ROR pre-treatment acts to either suppress the RWGS or reduce CO hold-up on the Ni surface. At 600 °C, over a prolonged time period, the 10% reduced samples exhibited rapid deactivation due to reactor blocking from carbon build up whilst the ROR pre-treated sample remained active over the 12 h time frame. The relative ease of CO desorption from the ROR samples results in less carbon formation from the Boudouard reaction. We have shown that ROR is effective for promoting Ni catalyst activity and selectivity. There remains scope for further optimisation of reduction conditions in order to minimise energy and product consumption. In addition, the potential exists for applying the ROR technique to a range of catalyst/support systems for the DRM as well as other heterogeneous catalyst systems.

#### Acknowledgements

The authors acknowledge the assistance of Dr Victor Wong as well as the expertise and equipment use from the UNSW Mark Wainwright Analytical Centre. Financial support from the Australian Research Council and the UNSW Faculty of Engineering are gratefully acknowledged.

#### Appendix A. Supplementary data

Supplementary data associated with this article can be found, in the online version, at <http://dx.doi.org/10.1016/j.apcatb.2016.05.080>.

#### References

- [1] A.T. Ashcroft, A.K. Cheetham, M.L.H. Green, P.D.F. Vernon, *Nature* 352 (1991) 225–226.
- [2] F. Wang, L. Xu, J. Zhang, Y. Zhao, H. Li, H.X. Li, K. Wu, G.Q. Xu, W. Chen, *Appl. Catal. B Environ.* 180 (2016) 511–520.
- [3] J. Huang, R. Ma, T. Huang, A. Zhang, W. Huang, *J. Nat. Gas Chem.* 20 (2011) 465–470.
- [4] H. Arbag, S. Yasyerli, N. Yasyerli, G. Dogu, *Int. J. Hydrogen Energy* 35 (2010) 2296–2304.
- [5] S. Damyanova, B. Pawelec, K. Arishtirova, J.L.G. Fierro, C. Sener, T. Dogu, *Appl. Catal. B Environ.* 92 (2009) 250–261.
- [6] W.D. Zhang, B.S. Liu, Y.P. Zhan, Y.L. Tian, *Ind. Eng. Chem. Res.* 48 (2009) 7498–7504.
- [7] D. Liu, R. Lau, A. Borgna, Y. Yang, *Appl. Catal. A Gen.* 358 (2009) 110–118.
- [8] S.B. Tang, F.L. Qiu, S.J. Lu, *Catal. Today* 24 (1995) 253–255.
- [9] M. Dan, M. Mihe, A.R. Biris, P. Marginean, V. Almasan, G. Borodi, F. Watanabe, A.S. Biris, M.D. Lazar, *React. Kinet. Mech. Catal.* 105 (2012) 173–193.
- [10] J.A. Lercher, J.H. Bitter, W. Hally, W. Niessen, K. Seshan, *Stud. Surf. Sci. Catal.* 101 (1996) 463–472.
- [11] M.C.J. Bradford, M.A. Vannice, *Catal. Rev.* 41 (1999) 1–42.
- [12] W. Chen, G. Zhao, Q. Xue, L. Chen, Y. Lu, *Appl. Catal. B Environ.* 136–137 (2013) 260–268.
- [13] P. Djinovic, I.G.O. Crnivec, B. Erjavec, A. Pintar, *Appl. Catal. B Environ.* 125 (2012) 259–270.
- [14] K.S. Hwang, H.Y. Zhu, G.Q. Lu, *Catal. Today* 68 (2001) 183–190.
- [15] J. Juan-Juan, M.C. Román-Martínez, M.J. Illán-Gómez, *Appl. Catal. A Gen.* 301 (2006) 9–15.
- [16] J. Juan-Juan, M.C. Román-Martínez, M.J. Illán-Gómez, *Appl. Catal. A Gen.* 264 (2004) 169–174.
- [17] Z. Hou, O. Yokota, T. Tanaka, T. Yashima, *Appl. Catal. A Gen.* 253 (2003) 381–387.
- [18] A.E. Castro Luna, M.E. Iriarte, *Appl. Catal. A Gen.* 343 (2008) 10–15.
- [19] V.M.V. Gonzalez-Delacruz, R. Pereniguez, R. Pere, F. Ternero, J.P. Holgado, A. Caballero, *ACS Catal.* 1 (2011) 82–88.
- [20] Y.-X. Pan, C.-J. Liu, P. Shi, J. *Power Sources* 176 (2008) 46–53.
- [21] S. Wang, G.Q. Lu, *Appl. Catal. A Gen.* 169 (1998) 271–280.
- [22] S. He, H. Wu, W. Yu, L. Mo, H. Lou, X. Zheng, *Int. J. Hydrogen Energy* 34 (2009) 839–843.
- [23] T.P. Kobylinski, C.L. Kirby, R.B. Pannell, E.L. Eddy, *Patent US4729981* (1986).
- [24] E.E. Unruh, L.H. Schwartz, J.B. Butt, *J. Catal.* 255 (1980) 242–255.
- [25] L. Tang, D. Yamaguchi, B. Leita, V. Sage, N. Burke, K. Chiang, *Catal. Commun.* 59 (2015) 166–169.
- [26] E. Lovell, Y. Jiang, J. Scott, F. Wang, Y. Suhardja, M. Chen, J. Huang, R. Amal, *Appl. Catal. A Gen.* 473 (2014) 51–58.
- [27] E. Lovell, J. Scott, R. Amal, *Molecules* 20 (2015) 4594–4609.
- [28] J.T. Feng, Y.J. Lin, D.G. Evans, X. Duan, D.Q. Li, *J. Catal.* 266 (2009) 351–358.
- [29] S. Velu, S.K. Gangwal, *Solid State Ionics* 177 (2006) 803–811.
- [30] C. Bartholomew, R. Pannell, *J. Catal.* 401 (1980) 390–401.
- [31] M.-S. Fan, A.Z. Abdullah, S. Bhatia, *ChemCatChem* 1 (2009) 192–208.
- [32] J.M. Ginsburg, J. Piña, T. El Solh, H.I. de Lasa, *Ind. Eng. Chem. Res.* 44 (2005) 4846–4854.
- [33] M.C.J. Bradford, M.A. Vannice, *Appl. Catal. A Gen.* 142 (1996) 73–96.
- [34] W. Jozwiak, E. Szubiakiewicz, J. Goralski, A. Klonkowski, T. Paryjczak, *Kinet. Catal.* 45 (2004) 247–255.
- [35] B. Mile, D. Stirling, M. Zammit, A. Lovell, M. Webb, *J. Catal.* 114 (1988) 217–229.
- [36] F. Pompeo, N.N. Nichio, M.G. González, M. Montes, *Catal. Today* 107 (2005) 856–862.
- [37] C.-S. Chen, J.-H. You, J.-H. Lin, Y.-Y. Chen, *Catal. Commun.* 9 (2008) 2381–2385.
- [38] D. Baudouin, U. Rodemerck, F. Krumeich, A. De Mallmann, K.C. Szeto, H. Menard, L. Veyre, J.-P. Candy, P.B. Webb, C. Thieuleux, C. Coperet, *J. Catal.* 297 (2013) 27–34.
- [39] S.-G. Wang, D.-B. Cao, Y.-W. Li, J. Wang, H. Jiao, *J. Phys. Chem. B* 109 (2005) 18956–18963.
- [40] J. Zhang, F. Li, *Appl. Catal. B Environ.* 177 (2015) 513–521.
- [41] C.L. Cheung, A. Kurtz, H. Park, C.M. Lieber, *J. Phys. Chem. B* 106 (2002) 2429–2433.
- [42] P.E. Anderson, N.M. Rodri, *Chem. Mater.* (2000) 823–830.
- [43] J.-H. Kim, D.J. Suh, T.-J. Park, K.-L. Kim, *Appl. Catal. A Gen.* 197 (2000) 191–200.
- [44] R. Martínez, E. Romero, C. Guimon, R. Bilbao, R. Martínez, *Appl. Catal. A Gen.* 274 (2004) 139–149.